θ_0 Angle of incidence of the mean ray on the multilayer. The axis of the second collimator makes an angle $2\theta_0$ with the mean incident ray.

θ Angle of incidence of a particular ray on the multilayer.

α Angle of incidence of the mean ray on the analyzer.

β Angle subtended by the crystallite which reflects the particular ray with the surface of the analyzer.

ϵ Angle of incidence of the particular ray on the crystallite at an angle β with the surface of the analyzer.

d_G Lattice spacing of the analyzing crystal.

References

CAGLIOTI, C., PAOLETTI, A. & RICCI, F. P. (1960). *Nucl. Instrum. Meth.* **9**, 195–198.

CAGLIOTI, C. & RICCI, F. P. (1962). *Nucl. Instrum. Meth.* **15**, 155–163.

CHOPRA, K. L. (1969). *Thin Film Phenomena*, pp. 11–25. New York: MacMillan.

COOPER, M. J. & NATHANS, R. (1968). *Acta Cryst.* A**24**, 481–484.

HAYTER, J. B., PENFOLD, J. & WILLIAMS, G. (1976). *Nature, Lond.* **262**, 569–570.

HILDEBRAND, F. B. (1956). *Introduction to Numerical Analysis*, pp. 323–326. New York: McGraw Hill.

JAMES, R. W. (1962). *The Optical Principles of the Diffraction of X-rays*, pp. 34–41. London: Bell.

LYNN, J. W., KJEMS, J. K., PASSELL, L., SAXENA, A. M. & SCHOENBORN, B. P. (1976). *J. Appl. Cryst.* **9**, 454–459.

MEZEI, F. (1976). *Commun. Phys.* **1**, 81–85.

RISTE, T. & OTNES, K. (1969). *Nucl. Instrum. Meth.* **75**, 197–202.

SAXENA, A. M. & SCHOENBORN, B. P. (1975). *Brookhaven Symposia in Biology*, No. 27, VII-30–VII-48.

SCHOENBORN, B. P., CASPAR, D. L. D. & KAMMERER, O. F. (1974). *J. Appl. Cryst.* **7**, 508–510.

SHULL, C. G. (1969). *Phys. Rev.* **179**, 752–754.

ZACHARIASEN, W. H. (1945). *Theory of X-ray Diffraction in Crystals*, pp. 123–135. New York: John Wiley.

ZINN, W. H. (1947). *Phys. Rev.* **71**, 752–757.

Acta Cryst. (1977). A**33**, 813–818

Correction Factors for Neutron Diffraction from Lamellar Structures

BY A. M. SAXENA AND B. P. SCHOENBORN

Biology Department, Brookhaven National Laboratory, Upton, NY 11973, *USA*

(*Received* 28 *January* 1977; *accepted* 11 *April* 1977)

In a spectrometer with finite beam divergence the vertical size of the reflections will increase with the order of reflection. This effect will be more pronounced if the mosaic width of the sample is large, which is often the case with biological samples. When the size of the reflection is greater than the detector size, a correction factor has to be introduced to account for this loss of intensity. A method of calculating this correction factor for a given beam divergence and mosaic width has been developed.

In recent years a number of neutron diffraction studies on biological membranes have been reported. These membranes have a lamellar structure with d spacing ranging from 50 to 300 Å. Some of these systems show a high degree of crystalline order with mosaic spreads of less than 0·3° (FWHM) like that found in lecithin cholesterol (Blasie, Schoenborn & Zaccai, 1975; Schoenborn & Blasie, 1975; Worcester, 1976). Other membranes often do not have good orientation and mosaic spreads of up to 60° have been reported for retinal rods (Yeager, 1975; Chabre, Saibil & Worcester, 1975). In this paper we will study the effect of vertical divergence of the neutron beam on the intensities of Bragg reflections for a sample with large mosaic distribution.

The main spectrometer characteristics influencing the intensities of Bragg reflections are: the diffraction geometry (Lorentz factor), the wavelength bandwidth $\Delta\lambda$ and the beam divergence $\Delta\theta$. The Lorentz factor accounts for the fact that different sets of crystal planes do not have equal opportunity to diffract the incident beam. For single-crystal rotation techniques this factor is a measure of the relative amounts of time spent by the corresponding reciprocal-lattice point in passing through the Ewald sphere and is equal to $1/\sin 2\theta$ for lamellar samples when the rotation axis is normal to the plane containing the incident and scattered beam (Arndt & Willis, 1966) where θ is half the scattering angle. The effective wavelength bandwidth $\Delta\lambda$ is determined by the mosaic characteristic of the monochromator and the beam divergence $\Delta\theta$ depends on various collimating slits. The effect of these two will be to smear the Ewald sphere. A neutron spectrometer differs in two important aspects from an X-ray spectrometer. Since the neutron flux is much lower, one has to work with greater $\Delta\lambda$ and $\Delta\theta$ to get observable intensities for weak reflections. Second, the neutron beam is monochromatized by reflection from a single crystal which leads to a correlation between the wavelength and diffraction angle from the monochromator. The result of this is that the resolution will depend on the constants of the spectrometer, the scattering angle and also the characteristics of the sample.

In order to determine an unknown structure, one

needs the relative intensities of various orders of reflection. In many cases it is possible to collect these intensities in such a way that the relative intensities are independent of the resolution function even though individual intensities are affected by it. For lamellar samples, however, the acceptance angle of the detector is important and needs special attention. With samples of large mosaic width, the vertical spread of reflections increases rapidly with the order of reflection, h, and the detector may not receive the entire diffracted beam. The fractional intensity received by the detector decreases with increasing h and a correction factor has to be introduced to take this loss of intensity into account.

The observed intensity of the hth-order reflection $I(h)$ is related to the corresponding structure factor $F(h)$ by the relation

$$I(h)=L_1L_2|F(h)|^2 \tag{1}$$

where L_1 is the correction term due to finite resolution of the spectrometer and the angular velocity factor, and L_2 is different from unity when the detector is not wide enough to receive the entire beam diffracted in the vertical direction.

For low-angle scattering, L_1 has generally been approximated to h and the total correction factor $L=L_1L_2$ is usually taken as h for samples with small mosaic and h^2 for samples with a large mosaic width. Chabre, Saibil & Worcester (1975) used a correction factor h in their work on oriented retinal rods in which data were collected with a 64×64 cm position-sensitive detector. Worcester (1976) and Worcester & Franks (1976) used the same correction factor in their work on lecithin and also for a study of purple membranes. Zaccai, Blasie & Schoenborn (1975) used a correction factor h^2 in a study of DPL where the FWHM of sample mosaic was 25°. Yeager (1975) originally used a correction factor of h^2 in a study of frog rod outer-segment disc membranes with a mosaic width of 60° but later took the detector acceptance angle into account.

It is obvious that the conclusions about a structure will be substantially influenced by the value assigned to the correction factor. Since $L=h^2$ is only an approximation for large mosaic distribution, it is necessary to develop a procedure by which the exact 'correction factor' may be calcuted for a given system.

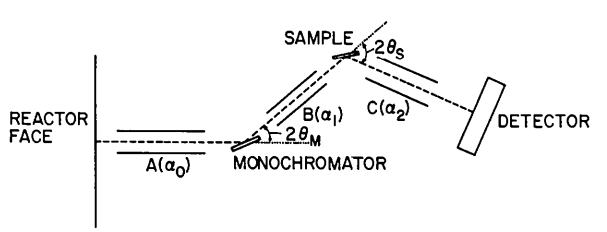

Fig. 1. Experimental setup for elastic neutron scattering. A, B and C are collimating slits with characteristic widths α_0, α_1 and α_2 respectively.

Lorentz factor L_1

The most convenient method of determining the structure of lamellar samples is to measure the intensity of rocking curves of different orders in which the detector is set to receive the reflection of a particular order and the sample is rocked about the Bragg position. Neglecting vertical divergence for the present, the intensity distribution in a rocking curve may be written as

$$I(\Delta\varphi)=I_0\exp\left[-\frac{(\Delta\varphi)^2}{2\sigma^2}\right], \tag{2}$$

where $\Delta\varphi$ is the angular deviation of the crystal from the optimum setting and I_0 is the maximum intensity of the reflection. σ is the characteristic width of the rocking curve, which will depend on the widths of the slits and the mosaic distributions of the monochromator and the sample. In writing (2), all these distributions have been assumed to be Gaussian in shape.

A typical experimental setup for a two-axis spectrometer is shown in Fig. 1. α_0, α_1 and α_2 are the characteristic widths of the three collimating slits. It is assumed that a ray making an angle θ with the axis of a slit is attenuated by the factor $\exp(-\frac{1}{2}(\theta/\alpha_i)^2)$ where $i=0$, 1, or 2. The mosaic widths of the sample and the monochromator are denoted by η_S and η_M respectively and are defined in an identical way. The probability of finding a mosaic block inclined at an angle β with the surface of the crystal is $\exp(-\frac{1}{2}(\beta/\eta)^2)$.

The net intensity of the rocking curve is obtained by integrating (2) over all values of $\Delta\varphi$. If this is combined with the angular velocity factor, the correction term L_1 may be written as (Iizumi, 1973)

$$L_1=\frac{1}{\sin 2\theta_B}\times\left[1+\frac{4\alpha_1^2\eta_M^2(a-1)^2+\alpha_0^2\alpha_1^2(2a-1)^2+4a^2\alpha_0^2\eta_M^2}{\alpha_2^2(\alpha_0^2+\alpha_1^2+4\eta_M^2)}\right]. \tag{3}$$

θ_B is the Bragg angle for the reflection in consideration and $a=\pm\tan\theta_B/\tan\theta_M$, where θ_M is half the scattering angle for the monochromator and the positive (negative) sign applies for parallel (antiparallel) setting of the monochromator and the sample. In (3) $1/\sin 2\theta_B$ is the usual angular velocity factor and the term inside the brackets represents the contribution due to finite resolution. Since a is a function of θ_B, the resolution correction will, in general, depend on h. However, if there is no slit between the sample and the detector, $\alpha_2=\infty$ and L_1 reduces to

$$L_1=1/\sin 2\theta_B. \tag{4}$$

Therefore the integrated intensity determined with an open detector of sufficient size will be independent of the resolution of the spectrometer. However, the correction factor L_1 will be important in cases where a Soller slit system is used.

Effect of vertical divergence

Since there is no correlation between wave number and direction of the neutron beam striking the monochromator, the reflected beam will be correlated only with respect to its horizontal divergence. This enables us to consider the vertical divergence independent of the distribution in the scattering plane. If a known intensity distribution in the vertical direction from the slit and a known mosaic distribution of the sample are assumed, the intensity distribution on the face of the detector can be calculated by convoluting these two functions.

While one is working with lamellar systems, it is advantageous to work with wide vertical slits because this exposes a greater area of the sample to the incident beam with a resultant gain in intensity of the diffracted beam. In such a setup the vertical divergence of the beam incident on the sample will be determined by the dimensions of the neutron beam pipe and the mosaic width of the monochromator. For the usual geometry the intensity distribution of the incident beam in the vertical direction can be closely approximated by the following function:

$$f_1(z)=\begin{cases} C_1 \exp\left(-\dfrac{(z+w/2)^2}{2\beta^2}\right) & \text{for } z\le -w/2 \\ C_1 & \text{for } |z|\le w/2 \\ C_1 \exp\left(-\dfrac{(z-w/2)^2}{2\beta^2}\right) & \text{for } z\ge w/2\,, \end{cases} \tag{5}$$

where z is in the vertical direction, w is the width of the central plateau region determined by the vertical slits and β is the characteristic width of the Gaussian curve forming the wings of the distribution which arises as a result of the divergence of the beam. The function f_1 is shown in Fig. 2. It follows from the geometry that

$$\beta=\varepsilon R \tag{6}$$

where ε is the angular divergence of the beam in the vertical direction and R is the distance of the detector from the sample. The requirement that the intensity under $f_1(z)$ remain constant with R leads to

$$C_1=C_1^0/(\sqrt{2\pi}\beta+w) \tag{7}$$

where C_1^0 is a constant, being equal to the net intensity on the sample. It follows from equations (5), (6) and (7) that the ratio of intensity under the plateau to that under the wings decreases as R increases.

If the distribution of mosaic blocks in the sample is Gaussian, a non-divergent point beam incident on the sample will give rise to the following intensity distribution at the detector:

$$f_2(z)=C_2 \exp\left[-\frac{z^2}{2\alpha^2}\right], \tag{8}$$

where α is the characteristic length of a reflection produced by a point source. If the mosaic width of the sample, η_{SV}, is large, the reflections will be in the shape of arcs and 2α will be the length of such an arc. It can be shown that to a good approximation

$$\alpha=2R\eta_{SV}\sin\theta_B\,. \tag{9}$$

The constant C_2 is determined by normalization and is given by

$$C_2=C_2^0/\sqrt{2\pi}\alpha\,, \tag{10}$$

where C_2^0 is proportional to the structure factor of the reflection at θ_B.

Let $I(z)$ represent the intensity distribution on the detector when the beam f_1 is incident on the sample. Then

$$I(z)=\int_{-\infty}^{+\infty} f_2(t-z)f_1(t)\mathrm{d}t\,. \tag{11}$$

This integration may be evaluated in a straightforward manner to give

$$\begin{aligned} I(z)=&\frac{\pi^{1/2}\alpha\beta C_1C_2}{[2(\alpha^2+\beta^2)]^{1/2}} \\ &\times\left[\exp\left\{\frac{-(w/2-z)^2}{2(\alpha^2+\beta^2)}\right\}\left\{1+\mathrm{erf}\left(\frac{\beta(z-w/2)}{\alpha[2(\alpha^2+\beta^2)]^{1/2}}\right)\right\}\right. \\ &\left.+\exp\left\{-\frac{(w/2+z)^2}{2(\alpha^2+\beta^2)}\right\}\left\{1-\mathrm{erf}\left(\frac{\beta(z+w/2)}{\alpha[2(\alpha^2+\beta^2)]^{1/2}}\right)\right\}\right] \\ &+\left(\frac{\pi}{2}\right)^{1/2}\alpha C_1C_2\left[\mathrm{erf}\left(\frac{w/2-z}{2^{1/2}\alpha}\right)+\mathrm{erf}\left(\frac{w/2+z}{2^{1/2}\alpha}\right)\right], \end{aligned} \tag{12}$$

where

$$C_1C_2=\frac{C_1^0C_2^0}{(2\pi)^{1/2}\alpha[(2\pi)^{1/2}\beta+w]}$$

and erf represents the error function defined by the following integral

$$\mathrm{erf}\,(x)=\frac{2}{\sqrt{\pi}}\int_0^x \exp\,(-u^2)\mathrm{d}u\,. \tag{13}$$

Physically speaking, the error function results from the convolution of the Gaussian function, f_2, with the plateau region of incident beam. The exponentials re-

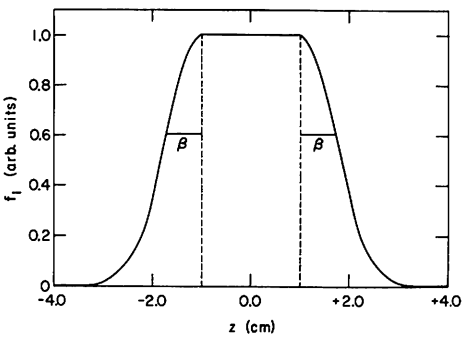

Fig. 2. Profile of the incident beam. The width of the central plateau is w and β is the characteristic width of the wings.

sult from the convolution of f_2 with the Gaussian portion of incident beam. In the special case when $w=0$, both f_1 and f_2 are Gaussian functions, and (12) simplifies to

$$I(z)=\frac{(2\pi)^{1/2}\alpha\beta C_1C_2}{(\alpha^2+\beta^2)^{1/2}}\exp\left\{-\frac{z^2}{2(\alpha^2+\beta^2)}\right\}, \quad (14)$$

which is also a Gaussian function, as expected. Also, if the beam divergence is negligible, $\beta=0$ and the distribution of intensity on the detector will be given by the last term of (12):

$$I(z)=\left(\frac{\pi}{2}\right)^{1/2}\alpha C_1C_2\left[\operatorname{erf}\left(\frac{w/2-z}{2^{1/2}\alpha}\right)+\operatorname{erf}\left(\frac{w/2+z}{2^{1/2}\alpha}\right)\right]. \quad (15)$$

If the detector slits extend from $z=-l$ to $z=+l$, the observed intensity will be obtained by integrating (12) over these limits:

$$I_D(2l)=\int_{-l}^{+l}I(z)\mathrm{d}z\,,$$

which gives

$$I_D(2l)=\frac{C_1^0C_2^0}{[(2\pi)^{1/2}\beta+w]}\int_{w/2-l}^{w/2+l}\left[\operatorname{erf}\left(\frac{t}{\sqrt{2}\alpha}\right)+\frac{\beta}{(\alpha^2+\beta^2)^{1/2}}\exp\left\{-\frac{t^2}{2(\alpha^2+\beta^2)}\right\}\times\left\{1-\operatorname{erf}\frac{\beta t}{\alpha[2(\alpha^2+\beta^2)]^{1/2}}\right\}\right]. \quad (17)$$

Therefore the correction factor for detector with vertical acceptance $2l$ is

$$L_2(h)=I_D(2l)/I_D(\infty)\,, \quad (18)$$

where $I_D(\infty)$ is the intensity obtained from (16) with $l=\infty$. It follows that for a detector large enough to receive the entire diffracted beam, $L_2=1$ and no correction is needed. The correction factor L_2 depends on η_S, R and θ_B only through α as given by (9).

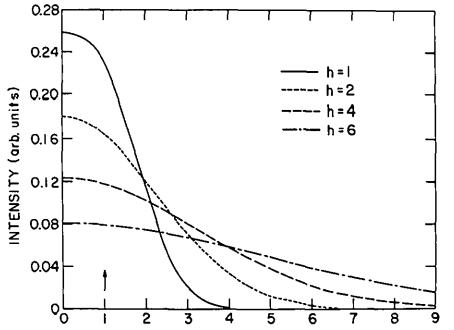

Fig. 3. Distribution of intensity on the face of the detector for $\eta_S=5{\cdot}0°$ and $w=2{\cdot}0$ cm. Intensities have been plotted for $h=1$, 2, 4, and 6, and have been normalized for equal total intensity. Therefore the peak intensity of a lower-order reflection is higher.

Fig. 3 shows a plot of $I(z)$, the distribution of intensity on the detector face as calculated from (12) for our experimental setup for a sample with $\eta_{SV}=5{\cdot}0°$. It can be seen that the reflections increase rapidly in size with increasing h, and a detector has to be more than 20 cm wide to receive the entire sixth order.

Equation (17) has been evaluated by Gauss's method of numerical integration. With the parameters of the spectrometer and the sample, L_2 may be calculated for each order of reflection. Since, the evaluation of this integral may be cumbersome, the correction factor $1/L_2$ has been plotted for the first eight orders for different values of sample mosaic in Fig. 4. In general, $1/L_2$ increases with increasing h or η_S, and even for $2l=6{\cdot}0$ cm it is appreciable for higher-order reflections. It may also be noted that $1/L_2$ does not increase linearly with h. A correction factor of h will therefore underestimate the contribution of higher-order reflections, while a correction factor h^2 will overestimate the contribution of higher-order reflections. It is important to evaluate this correction factor if the experiment deals with large values of η_{SV}, ε, or h. $1/L_2$ has been plotted in Fig. 4 with the assumption that the beam divergence, ε, is $1{\cdot}0°$ and the height of the incident beam, w, is 1·0 cm. These values are typical for an experimental arrangement for studying lamellar samples. However, if ε and w differ substantially from these values then the value of the appropriate correction factor cannot be obtained from Fig. 4. The deviation from the plots of $1/L_2$ will be more significant for small values of detector opening, $2l$, and large values of the order of reflection, h.

For small values of η_S and h the following simple algorithm gives a good first approximation to $1/L_2$ as calculated from (17): (1) Divide the slits (incident beam) into ten equal parts. (2) Assume that each part of the slit gives rise to uniform intensity over a length α as given by (9). This is equivalent to drawing a line of length α around each element. (3) The correction factor may be obtained from the part of these line elements intercepted by the slits.

If the width of a reflection is much greater than the opening of the detector slits, then one will essentially measure the peak intensity of the reflection. Substitution $z=0$ in (12) leads to

$$I_m=\frac{C_1^0C_2^0}{(2\pi)^{1/2}\beta+w}\left[\operatorname{erf}\left(\frac{w}{(8\alpha)^{1/2}}\right)+\frac{\beta}{(\alpha^2+\beta^2)^{1/2}}\exp\left\{-\frac{w^2}{8(\alpha^2+\beta^2)}\right\}\right]. \quad (19)$$

If we further assume that $w=0$, then (19) simplifies to

$$I_m'=\frac{C_1^0C_2^0}{[2\pi(\alpha^2+\beta^2)]^{1/2}}. \quad (20)$$

With α and β substituted from equations (9) and (6), this gives

$$I_m'=\frac{C_1^0C_2^0}{R\{2\pi[\varepsilon^2+(\eta_{SV}\lambda/d)^2h^2]\}^{1/2}}. \quad (21)$$

If $\eta_{SV}\lambda/d \gg \varepsilon$ the correction factor is simply $L_2 = 1/h$, which will apply only when the above condition is satisfied. In general, the value of the factor $1/L_2$ will lie between 1 and h.

Comparison with experiment

In order to compare these expressions with experimental results, one needs the parameters which appear in the functions f_1 and f_2 and the characteristic of the sample. The shape of the function f_2 may be studied by placing a narrow slit on the detector face and moving it vertically up and down to sample different sections of the beam profile. In our experiments a 17×17 cm position-sensitive detector (Alberi, Fischer, Radeka, Rogers & Schoenborn, 1975) was

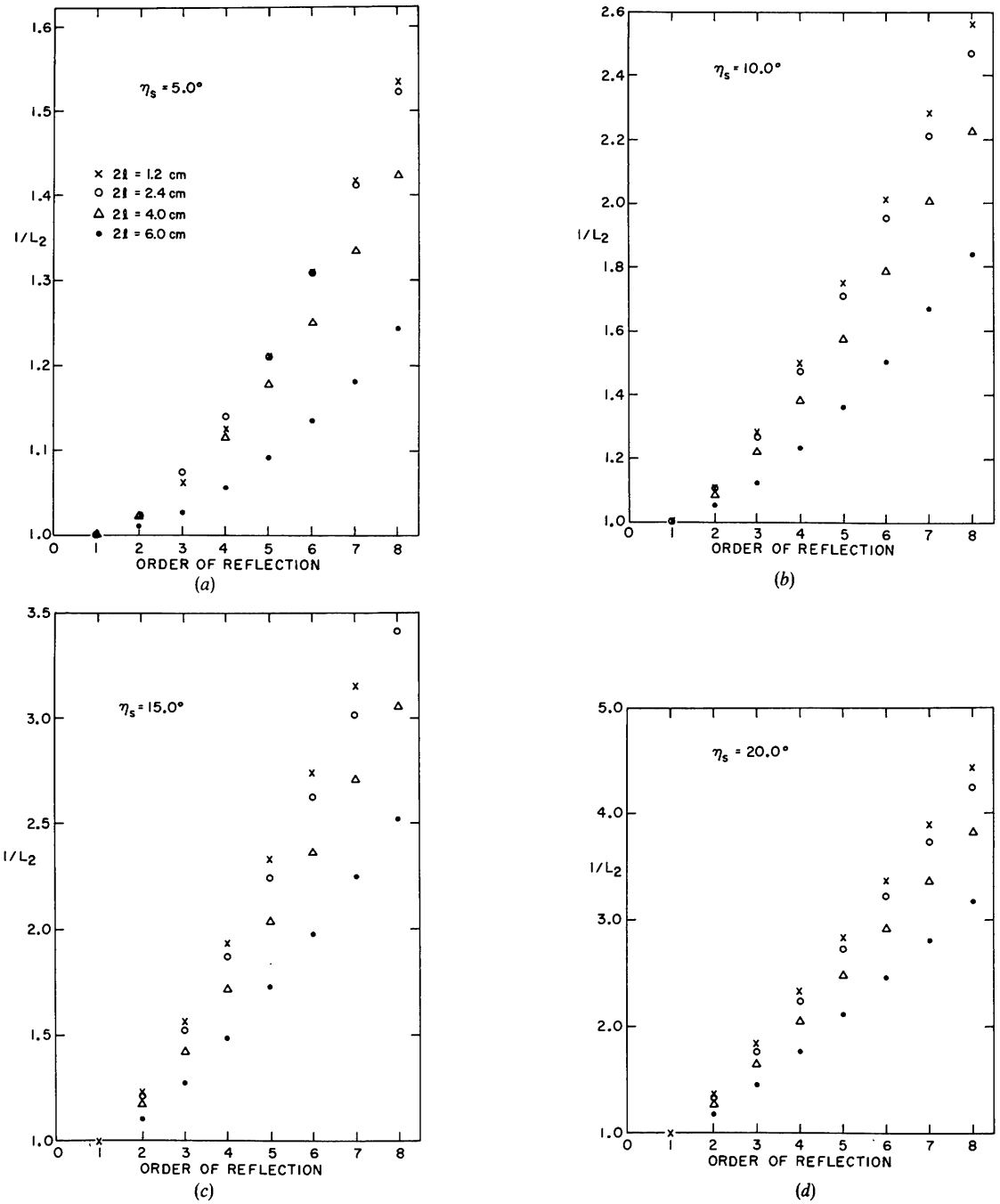

Fig. 4. Correction factor $1/L_2$ for the first eight reflections for $\eta_S = 5$, 10, and 20°. The parameters are: $R = 70$ cm, $\lambda = 2{\cdot}37$ Å, $d = 58$ Å, $\varepsilon = 1{\cdot}0°$, $w = 1{\cdot}0$ cm. $1/L_2$ has been plotted for four values of detector slits ($2l$): × 1·2 cm; ○ 2·4 cm; △ 4·0 cm; ● 6·0 cm.

used so that the beam profile could be directly observed. For this setup $L_1 = 1/\sin 2\theta_B$. If collimating slits are used before the detector, the value of L_1 will have to be calculated from (3) in terms of the constants of the spectrometer.

The shape of the function f_2 depends on the vertical mosaic width of the sample, η_{SV}. The value of this constant may be determined by taking a rocking curve of the sample with narrow collimation slits. If η_S is much greater than the characteristic widths of the collimating slits and η_M, then the width of the rocking curve is equal to η_S. However, if η_S is comparable to other characteristic widths, then all the widths will have to be determined with the help of a perfect single crystal, such as germanium. The value of η_S may then be found from the observed rocking curve and the known resolution function of spectrometer by following a procedure similar to that of Cooper & Nathans (1968). If the distribution of crystallites has a cylindrical symmetry about the normal to the sample, $\eta_{SH} = \eta_{SV}$ and the same measurement gives both the characteristic widths. For an asymmetric distribution of crystallites, η_{SV} may be determined by rotating the sample by 90° so that the original vertical direction lies in the scattering plane, and then analyzing the rocking curve.

Rocking curves of a DPL sample in the smectic phase were taken with the 17×17 cm detector. The mosaic width of the sample was determined to be 3·2°. Since the data were collected with a position-sensitive detector, the same set of data could be analyzed for different acceptance widths of the detector. The area of the rocking curves *vs* the detector opening is plotted in Fig. 5 for three orders of reflection. Each integrated intensity is normalized to the open-detector integrated intensity of the same reflection. It was found that a detector opening of 7 cm was sufficient to accept the entire diffracted beam from the fourth-order reflection. The agreement between the continuous curves calculated from (17) and the data points is very good.

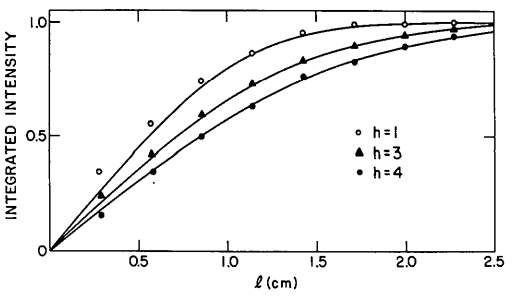

Fig. 5. Integrated intensity for different widths of detector slits. Open circles represent observed intensities for first-order reflection, solid triangles for third-order reflection and solid circles for fourth-order reflection. The continuous curves have been calculated from equation (17). Some systematic deviation for small values of l occurs for first-order reflections because the rocking curve for this order was not exactly Gaussian but had a greater concentration of intensity in the center.

Discussion

Owing to the vertical divergence of the beam, Bragg reflections from a sample with large mosaic spread will extend over large regions in the direction perpendicular to the scattering plane. This effect increases with the order of reflection, and for some biological samples the vertical spread may be 20 cm or more. If the detector is smaller than the size of the reflections, the correction due to this loss of intensity (which varies with the order of reflection) easily exceeds the statistical error in data collection and may substantially alter the analysis of the structure. Since linear detectors are being installed in a number of laboratories, a proper consideration of vertical divergence has become very important. Therefore it is worth while to determine the parameters of the sample and the spectrometer. The exact correction factor may then be evaluated for each reflection from the crystal.

Although we have considered Gaussian functions to represent f_1 and f_2, this procedure may be extended for any given function. If an experimental analysis shows that these functions differ substantially from the Gaussian shape then the appropriate shape functions may be substituted in (11) for the evaluation of the correction factor. A similar correction factor will apply when the diffraction data are collected by taking a θ–2θ scan of the crystal.

This research was carried out at Brookhaven National Laboratory under the auspices of the United States Energy Research and Development Administration. The authors are indebted to Drs M. Yeager and J. E. Cain for many useful discussions.

References

ALBERI, J., FISCHER, J., RADEKA, V., ROGERS, L. E. & SCHOENBORN, B. P. (1975). *IEEE Trans. Nucl. Sci.* **NS-22**, No. 1, 255–268.

ARNDT, V. W. & WILLIS, B. T. M. (1966). *Single Crystal Diffractometry*, pp. 279–288. Cambridge Univ. Press.

BLASIE, J. K., SCHOENBORN, B. P. & ZACCAI, Z. (1975). *Brookhaven Symp. Biol.* **27**, § III, pp. 58–67.

CHABRE, M., SAIBIL, H. & WORCESTER, D. L. (1975). *Brookhaven Symp. Biol.* **27**, § III, pp. 77–85.

COOPER, M. J. & NATHANS, R. (1968). *Acta Cryst.* A**24**, 481–484, 619–624.

IIZUMI, M. (1973). *Jap. J. Appl. Phys.* **12**, 167–172.

SCHOENBORN, B. P. & BLASIE, J. K. (1975). *Biophysics Congress*, August 4-9, 1975, Copenhagen, p. 379.

WORCESTER, D. L. (1976). *Biological Membranes*, edited by D. CHAPMAN, pp. 1–46. New York: Academic Press.

WORCESTER, D. L. & FRANKS, N. P. (1976). *J. Mol. Biol.* **100**, 359–378.

YEAGER, M. (1975). *Brookhaven Symp. Biol.* **27**, § III, pp. 3–36.

ZACCAI, G., BLASIE, J. K. & SCHOENBORN, B. P. (1975). *Proc. Natl. Acad. Sci. US*, **72**, 376–380.